THE JOURNAL OF PHYSICAL CHEMISTRY B

Article

pubs.acs.org/JPCB

# Prediction of Fundamental Properties of Ionic Liquid Electrospray Thrusters using Molecular Dynamics

Arnaud Borner, Zheng Li, and Deborah A. Levin*

Department of Aerospace Engineering, The Pennsylvania State University, University Park, Pennsylvania 16802, United States

**ABSTRACT:** Molecular dynamics (MD) simulations are performed to model an electrospray thruster for the ionic liquid (IL) EMIM−$BF_4$ using two coarse-grained (CG) potentials. Different equilibrium properties were obtained for the two potentials and then both were used to study the electrical extrusion of the IL for different electric field strengths and mass flow rates. The MD simulations provide the first insight into the atomistic modeling of a capillary-tip-extractor system, the basic elements of an electrospray thruster. One of the CG potentials was found to predict the formation of the Taylor cone, the cone-jet, and other extrusion modes for similar electric fields and mass flow rates observed in experiments of a IL fed capillary-tip-extractor system. Current distributions and anion and cation behavior were characterized and estimates of thrust and specific impulse are presented and compare reasonably well with measurements. Moreover, the role of inhomogeneities in the electric field as well as that of the IL space-charge most likely will improve agreement between modeling and experiment.

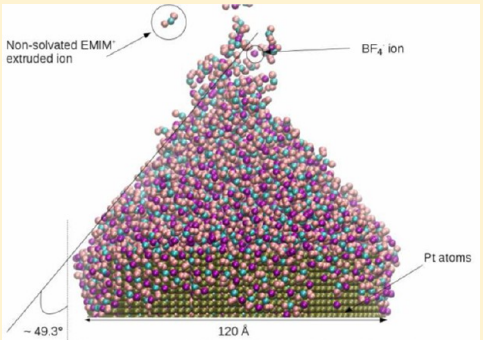

Taylor cone generated in a single cone-jet, pure ion mode.

## INTRODUCTION

Despite the existence for nearly 20 years of electrosprays in fields such as biomedical engineering, microelectromechanical systems, pharmaceutical development, food sciences, and industrial and aerospace engineering applications,[1,2] the physics of Taylor cone formation whereby a liquid surface is caused to deform under the presence of high electric fields[3] is still not completely understood. One important application of electrosprays is colloid thrusters[4−6] which can be used to provide small thrust levels with high specific impulse for satellite station keeping. Colloid thrusters (along with liquid metal ion sources[7] and field emission thrusters (FEEPs)) are a particular kind of electrospray. Different electrospray operation modes are possible, depending on the characteristic of the propellant such as its electric conductivity, surface tension, and dielectric tension, as well as the mass flow. It has been shown that the main operation modes exhibit electrospray structures known as dripping, microdripping, cone-jet, spindle, simple jet, or ramified jet,[8] although the focus of our studies are primarily of the cone-jet mode. The concept of generating propulsion from a liquid flow fed to the Taylor cone has been demonstrated by the presence of charged ions and droplets that are formed from the fragmentation of the jet downstream of the cone.[9] The cone-jet mode[9,10] can be further characterized by being in a pure ion mode, a pure droplet mode, or a mixed ion/droplet mode. The pure ion mode[11,12] is very attractive since it provides a higher specific impulse than most other electrospray operation modes, offering greater mission planning flexibility. It was discovered[13,14] that one propellant capable of operating in the pure ion mode at low temperature is the ionic liquid EMIM−$BF_4$, which will be discussed in this work. Ionic liquids (ILs) are characterized by a low temperature melting point (often under 100 °C). The low viscosity, low volatility and reusability of ILs are more reason that make them attractable as propellants as opposed to more traditional organic solvents.

A number of researchers have sought to model the physics of colloid thrusters using electrohydrodynamic approaches to model the cone-jet formation, with explicit assumptions to model the behavior of the fluid.[15,16] In ref 15, an axisymmetric colloidal jet model was used, with the liquid modeled as an incompressible viscous fluid with a constant conductivity. The equations were simplified by using a slenderness approximation, except for the free surface boundary conditions. In ref 16, the characteristic electrical relaxation time was assumed to be much shorter than any hydrodynamic time; hence, all of the electric charges were assumed to be confined to the free surface of the jet. These fluid models have provided important insights, however, the ultimate understanding of the physics of Taylor cone extraction is dominated by chemical interactions in the presence of strong electric fields at the atomistic level. Hence, molecular dynamics (MD) is the only approach that will provide the level of understanding and predictive capability required for the use of ILs as electrospray thrusters. MD simulations using all-atom potentials have been used to study the properties of ILs such as EMIM−$BF_4$. de Andrade et al.[17] computationally studied EMIM−$BF_4$ as well as other ILs by means of molecular mechanical and quantum *ab initio* calculations with a force field based on the AMBER methodology.[18] With respect to modeling of colloidal systems for propulsion applications, Takahashi and Lozano[19] studied the evaporation of solvated and nonsolvated ions of EMIM−

**Received:** February 28, 2013
**Revised:** May 8, 2013
**Published:** May 9, 2013

   dx.doi.org/10.1021/jp402092e | *J. Phys. Chem. B* 2013, 117, 6768−6781

$BF_4$ under high electric fields by using molecular dynamics (MD) simulations with the AMBER potential. However, these approaches are too computationally expensive to be extended to the scale of electrohydrodynamic approaches such as would be needed to characterize fundamental device performance.

This work proposes to offer the junction between the two approaches through the use of coarse-grained (CG) potentials in MD simulations. The use of CG potentials to model EMIM−$BF_4$ was first demonstrated by Daily and Micci[20] who estimated the ionic velocities and electrical conductivities of EMIM−$BF_4$ by using MD. They compared an all-atom model to two coarse-grained (CG) models, the simple coarse-grained and effective-force coarse-grained (EFCG)[21,22] models. In our previous work,[23] we demonstrated the use of a simple CG model to generate a complete electrospray by means of MD for EMIM−$BF_4$. Diffusion coefficients and electrical conductivities were calculated and showed good agreement with measured values and an electric field was applied to the system and the fraction, as well as the structures, of solvated and nonsolvated ions were analyzed.

A number of laboratory measurements on EMIM−$BF_4$ IL electrosprays have been made,[13,14,24,25] further making it a good candidate for fundamental MD studies. Romero et al.[13] investigated the currents produced by EMIM−$BF_4$ at room temperature for various flow rates. Ionic, droplet, and total currents were measured and it was discovered that this IL behaved differently from more classic propellants such as NaI/formamide since it could reach the pure ionic regime at ambient temperature due to its characteristics, mainly its conductivity and zero vapor pressure. The high volatility of the $EMIM^+$ ion was identified as the main reason why the purely ionic regime was easier to attain when EMIM−$BF_4$ was used compared to any other IL with similar characteristics. Chiu et al.[14] used time-of-flight/mass spectrometry to analyze the plume of an electrospray with EMIM−$BF_4$ and NaI/formamide as propellants. The electrospray was operated with positive and negative polarities. Pure ion emission was achieved with both polarities, and nonsolvated ions as well as two small-sized solvated ions were observed. A specific impulse in excess of 4000 s and an efficiency exceeding 90% were measured. Terhune and King[25] operated an EMIM−$BF_4$ electrospray thruster with negative polarity and measured the mass of the emitted ions with an ExB filter. They detected the three smallest anions and droplets of varying charges, attaining both the pure ion and mixed regimes.

Despite the significant modeling and laboratory studies a number of fundamental challenges still exist toward a complete understanding of the EMIM−$BF_4$, as well as ILs, in general. To-date, the conditions for the formation of a Taylor cone have not been predicted at the atomistic level by simulation. The Taylor cone can be both transient[26,27] as well as steady[9] in nature. Similarities and differences between steady cone-jets and transient jets formed in charged exploding drops were noted by de la Mora.[26] However, questions related to the difference between the structure of a transient jet formed on Coulombic fission and the steady cone-jet still remain.[28] The emphasis of our work therefore is to examine the formation of a steady state Taylor cone that has been repeatedly shown to form with a minimum flow rate by Fernandez de la Mora[9] and others.[11,24,29] To conduct an MD simulation of such a laboratory system, a reasonable scaling of the capillary radius and length as well as the emitter-to-extractor distance dimensions must be proposed. Finally, the MD system must be sufficiently large that a jet can be created, reach a steady state, and produce a sufficient number of ion-types to characterize the emitted jet structure and current types. This work will demonstrate that a sufficiently large system can be considered while maintaining a tractable computational cost by use of CG potentials.

With respect to the nature of EMIM−$BF_4$ specifically, a number of additional challenges are present. One of the reasons that EMIM−$BF_4$ is studied so extensively is that it is known to be an IL that easily reaches the pure ionic regime at ambient conditions but can also transition to a mixed ion/droplet regime at higher flow rates. Furthermore, a number of ILs have been found to follow the famous $I \propto Q^{1/2}$ law when operating in the droplet mode, where $I$ and $Q$ are the emitted current and mass flow rates, respectively.[9,29] EMIM−$BF_4$, however, does not follow this trend because of its rapid transition from pure ionic to mixed regimes at relatively low flow rates. In a purely ionic regime, Romero-Sanz[13] hypothesized that for a fixed q/m, the ion current versus mass flow trend must be linear. If we assume that only monomers are emitted, doubling the mass flow will result in a doubling of the current due to the monomers. However, we will show that for the cases studied here with EMIM−$BF_4$ as the IL of choice we rarely see the emission of a single ion type. Instead we see a combination of monomers, dimers and trimers in the purely ionic regime, or in an even more complicated mixed regime case, droplets and ions, with ions often being the result of a droplet breakup. Therefore, finding an analytical trend for the current versus mass flow is almost impossible since varying the mass flow means alternating between different emission regimes. Finally, the use of MD to predict the electric field and mass flow rate conditions for which EMIM−$BF_4$ exists in the ion versus droplet mode as well as whether the jet tends to break apart too quickly requires a molecular potential with high fidelity to represent the strong molecular interactions as well as an accurate representation of the electric field interaction with the IL. The latter factor will remain a limitation of the results presented here as will be discussed below.

Due to the complexity of the phenomena the use of semiempirical relationships to guide us in the formulation of MD simulations is important. Fernandez de la Mora and Loscertales[9] have shown that the cone-jet mode is attained when the volumetric flow lies between the limits

$$\frac{\gamma\varepsilon_0\varepsilon}{\rho Q} < Q < (\sim 20 \text{ to } 30) \times \frac{\gamma\varepsilon_0\varepsilon}{\rho K} \tag{1}$$

where $\gamma$ is the liquid surface tension, $\varepsilon_0$ is the permittivity of free space, $\varepsilon$ is the dielectric constant of the IL, $\rho$ is the density, $K$ is the conductivity and $Q$ is the volumetric mass flow. Using typical values for EMIM−$BF_4$ of $\gamma = 45.3 \times 10^{-3}$ kg/s$^2$, $K = 1.4$ S/m, $\rho = 1240$ kg/m$^3$, $\varepsilon = 12.2$, a volumetric flow rate between 2.93 and ∼70 pL/s, or in terms of mass flow rate $m$, between 3.63 and $\sim 84 \times 10^{-12}$ kg/s is obtained. The electric current and the average diameter of the droplets ejected by cone jets have been reported in a variety of publications. The scaling laws for $I$ and $D_d$ are[9,10]

$$I = f(\varepsilon)\left(\frac{QK\gamma}{\varepsilon}\right)^{1/2} \tag{2}$$

and

$$D_d = g(\varepsilon)\left(\frac{Q\varepsilon\varepsilon_0}{K}\right)^{1/3} = g(\varepsilon)r^* \tag{3}$$


dx.doi.org/10.1021/jp402092e | J. Phys. Chem. B 2013, 117, 6768−6781

where $g(\varepsilon)$ is an empirical factor of order unity, and $r^*$ is a characteristic length scale for the radius of the jet near its base

$$r^* = \left(\frac{Q\varepsilon\varepsilon_0}{K}\right)^{1/3} \quad (4)$$

Using the values for EMIM−$BF_4$ relative to our computations, the jet was expected to have a radius $r^*$ on the order of 40−110 Å depending on the mass flow rate used. By using eq 2, the average specific charge for emitted droplets of a colloid thruster, which is the main parameter of interest rather than their droplet diameter, can be computed as

$$\left\langle \frac{q}{m} \right\rangle = \frac{I}{\rho Q} \approx \left[\frac{f(\varepsilon)}{\rho}\right]\left(\frac{K\gamma}{Q\varepsilon}\right)^{1/2} \quad (5)$$

Using these relationships as a starting point, the objective of this work is to explore the atomistic representation of the cone and cone-jet flow extracted from a capillary-emitter-extractor system. Initially, we present the simple CG molecular potential used in our previous work[23] and a higher fidelity effective-force coarse grained (EFCG) potential as well as the equilibrium properties predicted by these potentials. To create a mass flow rate inside the capillary, we introduce the use of a moving potential wall. The sensitivity of the MD simulation results to the intermolecular potential model is investigated. Specifically we examine the difference in the predicted jet structure and currents in both the pure ion and mixed ion-droplet mode as a function of extraction electric field and mass flow rates and compare our MD predictions with experiment. We demonstrate that the Taylor cone structure is predicted by the EFCG model to occur under the conditions observed in experimental observations. Values for the thrust and impulse are estimated as well. In the Conclusions and Future Work section, the need in future work to model the spatially inhomogeneous electric field as well as the effect of space-charge are emphasized.

## MOLECULAR DYNAMICS MODELS

**Comparison of Equilibrium Properties Predicted by Two Coarse-grained Models.** Similar to our previous work,[23] a coarse-grained (CG) model of the ionic liquid (IL) EMIM−$BF_4$ was used to achieve a significant decrease in the computational cost compared to an all-atom model. The use of a coarse-grained model allows one to simulate a much larger system with respect to the number of ion pairs, for the same computational cost, when compared to a full-atom model. The coarse-grained model gives a reduction in the total number of groups per ion pair from 25 to 5. Since the emphasis of this work is on replicating experimental results, the size of the system is much more important than the very subtle differences between all-atom and coarse-grained models. In this work, we investigate two different coarse-grained models in order to understand the dependence of the IL spray modeling on the potential. The coarse-grained potentials mainly differ in their treatment of the intramolecular potential of the cation, $U_{intra}$, where the total potential is the sum of that term and intermolecular potentials, $U_{inter}$. First we consider the simple coarse-grained (simple CG) potential presented in ref 23. In this model, the EMIM+ cation is represented as a rigid model ($U_{intra} = 0$) and the interactions between the different groups ($U_{inter}$) were modeled as the sum of Lennard-Jones 12−6 and Coulomb interactions. The potential parameters for the simple CG potential are summarized in Table 1, while the bond lengths and angles are depicted on Figure 1a. The $EMIM^+$ ion was modeled as a rigid body in the simple CG approach. One way to define a rigid molecule involves imposing a sufficient number of bond constraints between the atoms in the unit. However, the particular geometry of the $EMIM^+$ ion in the simple CG approach (the M1, IM and MR groups are aligned) make it problematic to define a sufficient number of bond constraints. Also, problems with the stability and speed of the RATTLE[30] often arise when constraints are used. The use of rigid body units, whose dynamics are defined by translation of the center of mass and rotation about it, allows one to avoid these problems. It is common practice to define the position of the body in a universal frame of reference, but to describe the moment of inertia tensor in a frame of reference that is localized in the rigid body and changes as the rigid body rotates. The orientation of the local body frame with respect to the space fixed frame is described via a four dimensional unit vector called the quaternion. The equations of the translational motion of a rigid body are the same as those describing the motion of a single atom, except that the force is the total force acting on the rigid body and the mass is the total mass of the rigid body unit.

**Table 1. Lennard-Jones and Coulomb Parameters for the Simple Coarse-grained Model[a]**

| group | mass (g/mol) | $q$ | $\sigma$ (Å) | $\varepsilon$ (kcal/mol) |
|---|---|---|---|---|
| M1 | 15.03 | +0.22 | 2.90 | 0.157 |
| IM | 67.07 | +0.4795 | 2.77 | 0.643 |
| MR | 14.03 | +0.2112 | 2.90 | 0.141 |
| M2 | 15.03 | +0.0871 | 2.90 | 0.157 |
| $BF_4$ | 86.81 | −1 | 3.05 | 0.339 |

[a]The charge distribution, $q$, is the same for both the simple and EFCG potentials.

The second potential model used in this study is the effective-force coarse-grained (EFCG) potential, proposed by Wang et al.[22] for the $EMIM^+NO_3^-$ IL system. The EFCG potential uses a modified AMBER[18] force field form to represent the intramolecular potential,

$$U_{intra} = U(r) + U(\theta)$$

where the contribution due to dihedral interactions was found to be negligible and therefore removed from this model. Bond and angle parameters used in the EFCG model are summarized in Table 2 and Table 3, while the bond lengths and angles are depicted on Figure 1b. To reproduce the local structure of an all-atom model, the nonbonded interactions, $U_{inter}$, consisting of both Coulomb (see Table 1) and van der Waals forces were constructed by Wang et al.[22] The translational force between two atomic groups was computed and projected onto the radial vector between the center of masses of these two atomic groups and the resulting force−distance relation was tabularized for input into the MD code. Supporting Information was provided by Daily.[31] All MD calculations were performed using a modified version of DL_POLY.[32]

Preliminary calculations were done to investigate the behavior of both potentials at ambient temperature by placing 270 EMIM−$BF_4$ pairs in a cubic box of size 41.4 Å, so that the initial density of the system was about 1240 kg/$m^3$, the experimentally measured value at 295 K and atmospheric pressure. Periodic boundary conditions were applied in all three directions, and the temperature and pressure were set to 295 K and 1 atm, respectively. Two separate simulations were carried


dx.doi.org/10.1021/jp402092e | J. Phys. Chem. B 2013, 117, 6768−6781

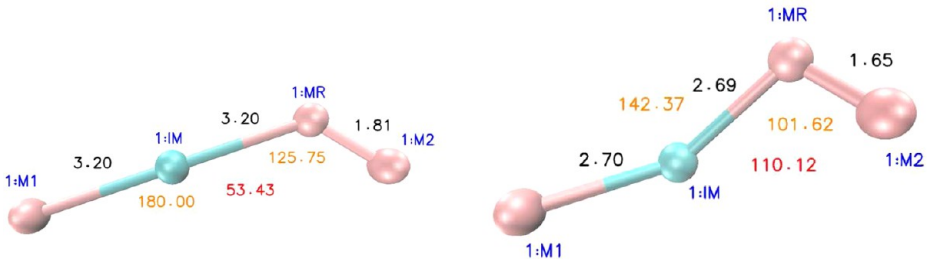


(a) Simple CG potential model. (b) EFCG potential model.

**Figure 1.** Coarse-grained structure for the 1-ethyl-3-methylimidazolium ionic liquid. The group name is displayed in blue, the bond length in black (units = Å), the bond angle in orange (units = deg) and the dihedral angle in red (units = deg). Note that the bonds of the molecule for the EFCG potential are slightly stretched, hence why they are different from the equilibrium values provided in Table 2 and Table 3.

**Table 2. Bond Parameters 4for the EFCG potential $U(r) = (k/2)(r - r_0)^2$**

| bond | $k$ (kcal/mol) | $r_0$ (Å) |
|---|---|---|
| M1−IM | 421.5 | 2.71 |
| IM−MR | 438.7 | 2.69 |
| MR−M2 | 346.6 | 1.66 |

**Table 3. Angle Parameters for the EFCG Potential $U(\theta) = (k/2)(\theta - \theta_0)^2$**

| bond | $k$ (kcal/mol) | $\theta_0$ (°) |
|---|---|---|
| M1−IM−MR | 227.9 | 142.383 |
| IM−MR−M2 | 136.5 | 109.446 |

for each CG potential model, one in an NVT ensemble using a Nose-Hoover[33,34] thermostat to generate the radial distribution functions and the other one in the NPT ensemble using a modified Nose-Hoover barostat[35,36] to determine the equilibrium density. The thermostat relaxation constant was always set to 30 fs for both the NPT and NVT simulations, while the barostat relaxation constant was set to 400 fs in the NPT ensembles. A time step of 2 fs was used and the system was equilibrated for 600 fs, then the NVE production runs lasted a further 400 ps, so that the total run time was 1 ns. For the NVT simulations, the velocities were rescaled every 5 timesteps during the equilibration phase. Cutoffs for the short-range van der Waals interaction and the real part of the long-range Coulombic interaction were chosen to be respectively 12 and 20 Å. The Smoothed Particle Ewald Sum (SPME) method,[37] which is a modification of the basic Ewald sum,[38] was used to calculate the electrostatic interactions. The main difference between the methods is in the treatment of the reciprocal space terms.

Densities were calculated from the final volume of the NPT simulation at atmospheric pressure. For the simple CG potential, the density averaged over the production run was 2508 kg/m$^3$, or twice as large as the initial value. For the EFCG potential, the density averaged over the production run was 1220 kg/m$^3$, or a 1.6% error when compared to the initial value. Radial distribution functions (RDF) were computed from the NVT simulation and are shown in Figure 2a−c. The position of the peaks in the RDFs obtained from the simple CG potential match the ones obtained by Daily and Micci,[20] however, a number of discrepancies with those obtained from the EFCG potential can be seen. The RDFs obtained from the EFCG potential compare very well with the ones obtained by de Andrade et al.[17] and del Popolo and Voth[39] for the all-atom models, and Wang et al.[22] for both the all-atom and EFCG models. The RDFs show that the different groups are closer to each other in the simple CG than in the EFCG and all-atom models, which would explain why the density of the system at equilibrium was double the value measured experimentally. Figure 3a and b shows a snapshot of the final configuration of the system for the NVT simulation for both potentials. It can be seen that due to the use of periodic boundary conditions and the fact that the box was dimensioned to accommodate a density of 1240 kg/m$_3$, a spurious "bubble" was formed in the

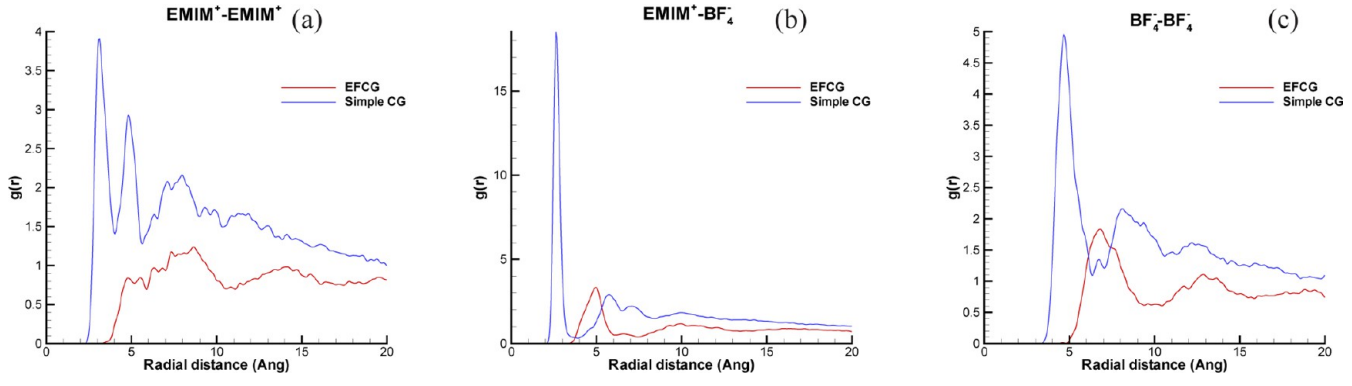


**Figure 2.** RDFs for the simple and effective-force coarse-grained models.


dx.doi.org/10.1021/jp402092e | J. Phys. Chem. B 2013, 117, 6768−6781

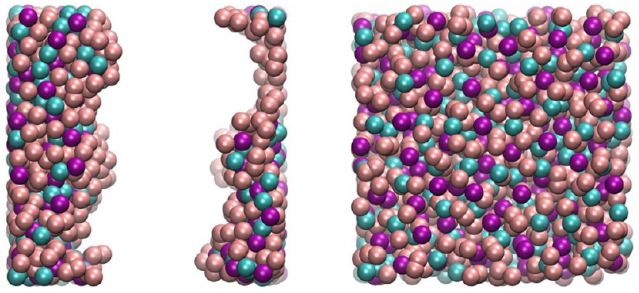

Figure 3. Snapshot of the final configuration during the equilibration of a box with PBC containing 440 EMIM−$BF_4$ in the NVT ensemble.

middle of the box for the simple CG potential. These preliminary calculations suggest that the EFCG potential is better designed to represent the equilibrium characteristics of EMIM−$BF_4$, whereas the simple CG potential may not. Since our main goal is to look at IL systems under nonequilibrium conditions, we also examine the cone/jet system using the simple CG potential but consider the EFCG the baseline potential.

**Equilibration in a Capillary Geometry, Prior to Extrusion.** Following these preliminary calculations, a system of 9455 EMIM−$BF_4$ ion pairs were placed in a crystal structure inside a capillary composed of 16626 Pt atoms. The system size was chosen as a compromise between the computational cost and the minimum capillary diameter with a cylinder height to radius ratio of about five to preserve the capillary needle shape. The inside radius and length of the capillary were chosen to be respectively 56 and 275 Å, so that the initial density of the system would be once again 1240 kg/m$^3$, consistent with values predicted for $r^*$ by eq 4. Periodic boundary conditions were applied in the longitudinal direction only since the system had a cylindrical geometry. Interactions between the IL and the Pt atoms were modeled by simple Lennard-Jones 12−6 interactions. The electrostatic interactions in the IL were calculated by using the force-shifted Coulomb sum,[40] since the use of the Ewald summation is restricted to 3D periodic systems only in DL_POLY. It was found that a time step of 5 fs provided the same accuracy as a time step of 2 fs for both potentials. The system was equilibrated for a total duration of 0.5 ns and was rescaled every 5 time steps for 0.25 ns in the NVT ensemble at 295 K using the Nose-Hoover thermostat with a relaxation constant of 30 fs. The system was equilibrated a further 0.25 ns in the NVE ensemble and the temperature variations were monitored and judged acceptable since they were under 1%. The equilibrated system obtained using the EFCG potential showed a homogeneous distribution inside the Pt capillary, while the system obtained after equilibration when using the simple CG potential agglomerated around the axis of the cylinder, forming a bulk of IL with a density close to the one obtained for that potential during the preliminary calculations discussed previously. A new Pt capillary was therefore created around the cylinder of IL to ensure that no vacuum was present between the IL and the Pt wall. That system was ran a further 0.1 ns to take into account the new interactions created by the new, closer positions between the Pt atoms and the outer layer of IL ions.

The use of periodic boundary conditions in the longitudinal directions for the equilibration meant that some $EMIM^+$ ions were split between the two periodic boundaries of the domain. Since these periodic conditions were lifted during the extrusion production computations, these split ions were removed at the end of the equilibration. The systems then became negatively charged, and some $BF_4^-$ ions were expelled from the capillary due to a strong repulsive Coulomb interaction between negative charges. These ions were tracked down and also removed from the system. The final systems before the production runs were started had the following size for the EFCG and simple CG potentials: 9341 and 9149 cations, and 9455 and 9411 anions, respectively.

**Extrusion Model.** To generate a mass flow inside the capillary, a moving potential wall was created by generating a strong short-ranged repulsive force. The moving potential wall is based on a modified (9−3) inverse power function[41,42] and defined as follow:

$$\phi_{\text{wall}}(z) = \begin{cases} -\frac{\varepsilon_{\text{wall}}}{2}\left[\left(\frac{3}{z-(z_0+v\times\Delta t)}\right) - 3\left(\frac{3}{z-(z_0+v\times\Delta t)}\right)\right] & z < 3\ \text{Å} \\ 0 & \text{otherwise} \end{cases} \quad (6)$$

where $z$ is the distance between the wall and a particle, $z_0$ is the initial wall position, $v$ is the wall velocity, $\Delta t$ = 5 fs is the time step, and $\varepsilon_{\text{wall}}$ = 0.1195 kcal/mol. The force generated by the moving wall potential is applied only to particles that are located inside the Pt capillary. It can be seen from this equation that the repulsive wall only affects particles that are within a 3 Å distance. This displaced the ionic liquid inside the capillary giving it a constant velocity and therefore simulating the liquid displacement with a constant mass flow. Figure 4 shows the displacement of the wall between the initial time and a time later in the push process.

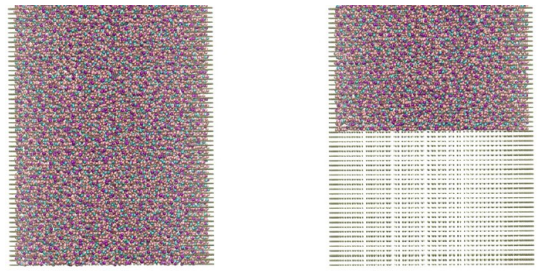

Figure 4. Displacement of the moving potential wall. Vertical dimension corresponds to 150 Å.

A constant positive electric field $E_z$ was applied in the longitudinal direction **z**, outside of the Pt capillary, generating an electric force of the form

$$\mathbf{F}_{e_{x,y}} = \mathbf{0} \quad (7)$$

$$\mathbf{F}_{e_z} = qe\mathbf{E}_z \quad (8)$$

where $F_e$ is the electric force, $e$ is the elementary charge and $q$ is the partial charge of a group.


dx.doi.org/10.1021/jp402092e | J. Phys. Chem. B 2013, 117, 6768−6781

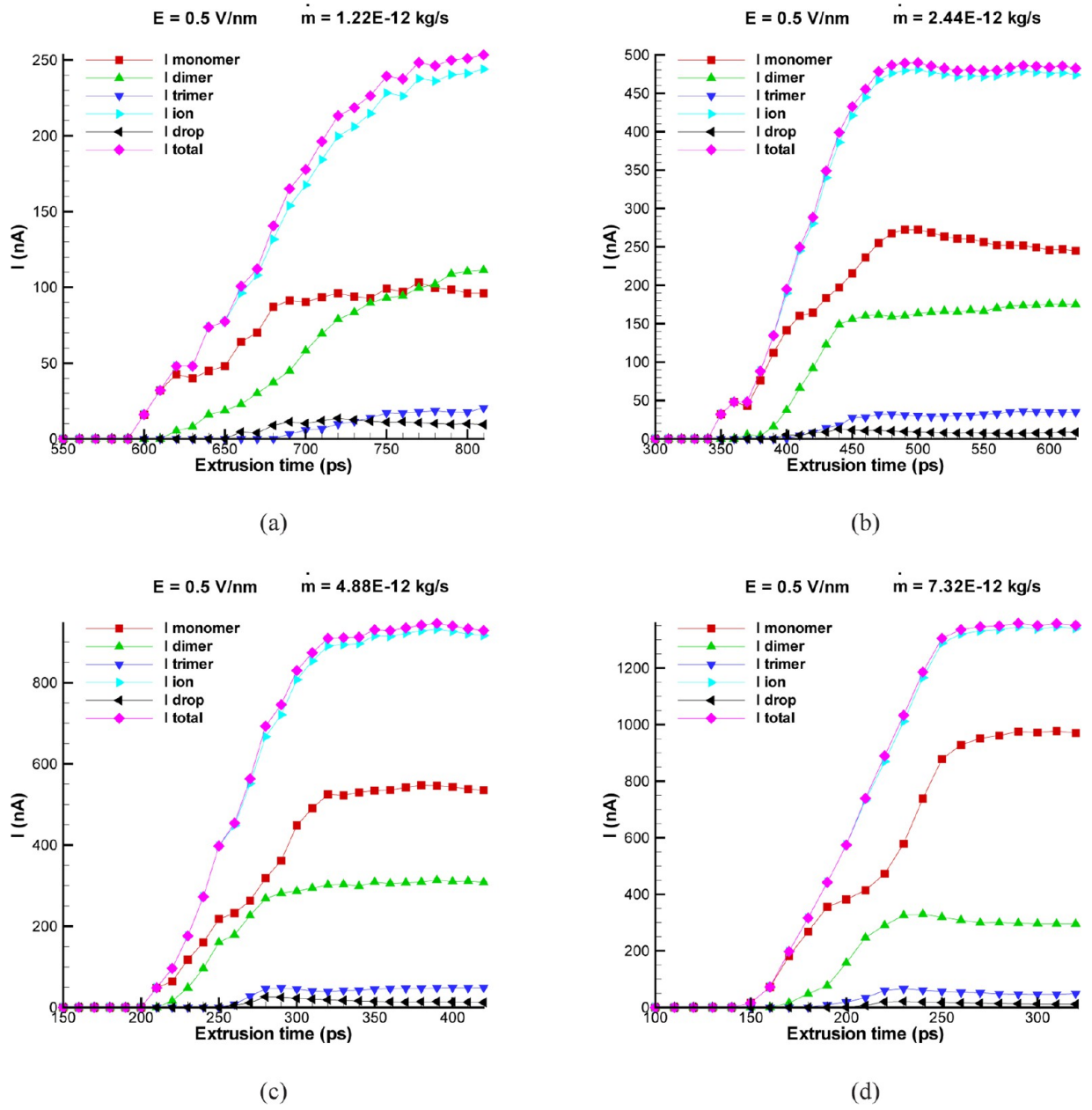


**Figure 5.** Comparison of currents as a function of the extrusion time, for the EFCG potential model for an applied electric field of 0.5 V/nm and different mass flow rates.

## RESULTS AND DISCUSSION

For both molecular potentials the IL mass flow rates were varied between $0.61 \times 10^{-12}$ and $48.8 \times 10^{-12}$ kg/s, consistent with eq 1 and spatially uniform electric field strengths of 0.5, 1.0, and 2.0 V/nm were applied to the equilibrated IL-capillary system. The range of electric field values of 1 to 2 V/nm was selected based on our previous work[23] and the lower value of 0.5 V/nm was selected because the use of Taylor's relationship[3] for an EMIM−$BF_4$ droplet gives a critical electric field required to initiate direct ionization on the order of 0.5 V/nm.[20] Statistics of emitted ions and current were calculated from the MD simulations at a distance 0.1 $\mu$m away from the center of the capillary, or 862.5 Å from the tip of the capillary, simulating the position of an extractor, a ring at one of the three aforementioned voltages biased with respect to the capillary tip. The upper lip of the green cylinder in Figure 6a will be referred to as the "tip of the capillary" from this point onward. The "center of the capillary" is the actual barycenter of the green cylinder, not visible in Figure 6a. Comparison of these dimensions with the value of $r^*$ given by eq 4 shows that for the mass flow rates considered here the MD simulation domain is sufficiently large to capture the physics of electrospray extrusion discussed in many laboratory experiments.[11−14,24,25,43,44]

Since currents of single and clusters of ions are important measurements for characterizing the physics of ion emission as well as providing estimates of colloid thruster performance, these values were crucial metrics that we wanted to obtain from the MD simulations. A postprocessing algorithm was developed to analyze the MD trajectories by recording cluster size and charge when an ion or cluster reached the virtual extractor. Ion clusters have the form of aggregates of $(EMIM^+BF_4^-)n$


dx.doi.org/10.1021/jp402092e | J. Phys. Chem. B 2013, 117, 6768−6781

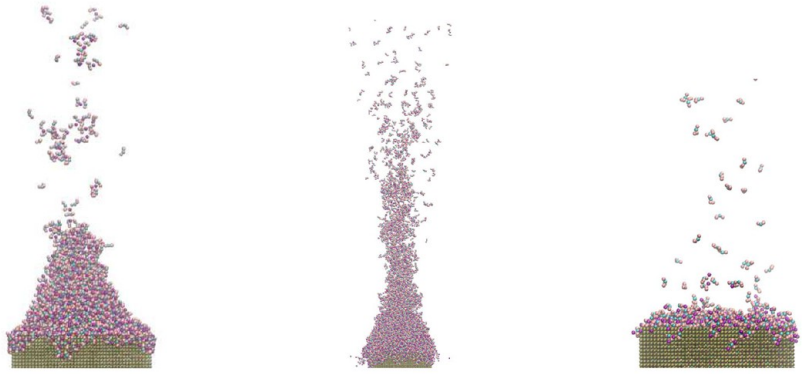


**Figure 6.** IL flow structures obtained from the MD simulations for the EFCG potential. Green spheres represent Pt capillary atoms, red spheres represents M1, MR and M2 groups, green-blue spheres represent the IM groups whereas purple spheres represent $BF_4^-$ ions. (a) Taylor cone generated in a single cone-jet, pure ion mode, with entire domain shown, vertical dimension of 330 Å. (b) Entire domain showing the well-defined structure of the cone-jet, vertical dimension of 655 Å. (c) Close-up view of multi cone-jet mode operation, vertical dimension of 190 Å.

$(EMIM^+)$ or $(EMIM^+BF_4^-)n$ $(BF_4^-)$ where $n$ = 0,1,2... for negative and positive voltages, respectively and $n$ = 0 represents pure ion or nonsolvated ions. Charged clusters with values of $n \geq 9$ are designated as droplets. To determine whether neighboring ions belong to the same cluster, a neighbor list is created for each ion and the list was searched for all other ions to determine which ones lie within a sphere of radius 8 Å centered at its center of mass. The 8 Å cutoff was chosen based on observations made of our RDF plots, as well as those from Daily and Micci,[20] which show that, statistically, most of the ions forming a cluster are separated by a distance less than that cutoff.

During the MD simulations it is generally seen that charged clusters with an overall positive charge travel to the virtual extractor (biased negative relative to the capillary tip) when the positive operation mode is simulated. Negatively charged clusters never reach the virtual extractor due to the positive electric field. Neutral clusters are created by in-flight fragmentation of larger droplets and can also reach the virtual extractor by their momentum after fragmentation. Figure 5 shows the different measured currents as a function of the extrusion time for an applied electric field of 0.5 V/nm and different mass flow rates. using the EFCG potential model and the moving wall potential described by eq 6. The calculation of current starts when the first cluster reached the virtual extractor. The time prior to any charged particles reaching the extractor may be interpreted as a relaxation time which can be seen from the figure to decrease (from 590 to 340 to 200 to 150 ps) as the mass flow rate increases (from 1.22 to 2.44 to 4.88 to 7.32 × $10^{-12}$ kg/s). It can also be seen that the time to obtain steady state current values decreases with increasing mass flow rate, as expected. Note that the current values reported in subsequent figures are the steady state values that were calculated after the transient phase of current initialization. As will be discussed in more detail below, the computed results in Figure 5 show good agreement with the experimental results of Romero-Sanz et al.[13] who measured ionic currents of monomers $(EMIM^+)$, dimers $[(EMIM{-}BF_4)EMIM^+]$, and trimers $[(EMIM{-}BF_4)_2EMIM^+]$ of $EMIM{-}BF_4$ at 24 °C and found that the contribution of other ions to the total ionic current was mostly negligible.

**Results Obtained Using the EFCG Potential.** *The Positive Operation Condition.* First we consider the structure of the IL flow as it leaves the capillary under the extrusion of the external field. Figure 6a shows the flow in the region of the capillary tip for an extraction field of 0.5 V/nm. Under similar conditions, measurements[13,44] and theory[9] predict the formation of a single, Taylor cone-jet flow in the ion mode. The cone half angle can be estimated from Figure 6a to be very close to the value proposed by Taylor[3] of 49.29° which is independent of the type of IL, the field, or the mass flow rate. Examination of the "jet" portion of the flow shown in Figure 6a for an electric field of 0.5 V/nm and a mass flow rate of 1.22 × $10^{-12}$ kg/s shows that small ions are emitted from the tip of the Taylor cone at this low flow rate. However, if the mass flow rate is increased (Figure 6b), the Taylor cone with a sustained jet structure can be clearly seen. The Taylor-cone and the cone-jet structure have been readily observed in numerous experiments, but this represents the first time, to our knowledge, that it has been predicted in an MD simulation for a flowing liquid.

To compare the change in the extrusion physics for different extraction voltages and mass flow rates, it is useful to compare the predicted magnitude and type of charged particle currents with measurements. Figure 7 shows the different currents computed for an electric field of 0.5 V/nm at varying mass flow rates. Note that in the figure each closed symbol represents the MD steady state current, as determined from Figure 5. The first general trend that can be seen is that most currents increase with increasing mass flow in both the MD simulations and data. The generally larger MD magnitudes may be due to the fact that the constant electric field is assumed to be only along the longitudinal axis. The trimer and droplet currents closely match the value measured by Romero-Sanz (Figure 7c), while the dimer current matches the measured values for most mass flow rates except those greater than 15 × $10^{-12}$ kg/s, as shown in Figure 7b. The computed monomer current tends to increase more quickly than the values measured by Romero-Sanz (Figure 7d). This discrepancy deserves further discussion.

We believe the larger droplets emitted from the cone-jet have a tendency to break apart that is higher in our simulations than it actually is in experiments, such as the one conducted by Romero-Sanz et al.[13] Romero-Sanz et al.[13] reports that few droplets break apart when traveling from the tip of the jet to the current collector and that ion evaporation from drops in-flight is not significant for $EMIM{-}BF_4$. The tendency of our simulations to over predict droplet break up may be due to the

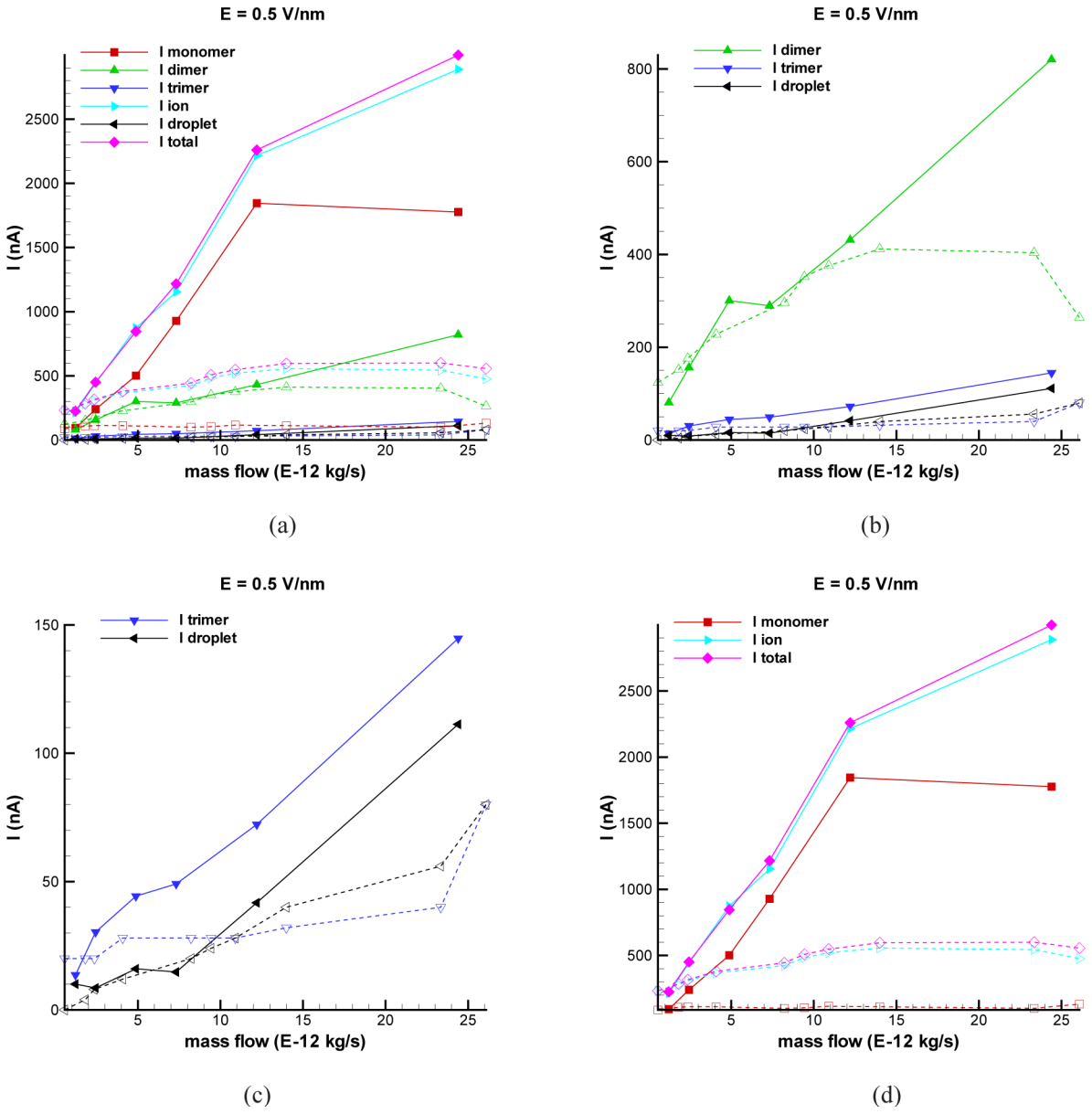


**Figure 7.** Currents as a function of the mass flow rate for the EFCG potential model and applied electric field of 0.5 V/nm. Solid lines represent the calculated currents while dashed lines represents the measured current values from Romero-Sanz et al.[13]

fact that our model simulates a constant, spatially homogeneous electric field, with a value chosen to be at least equal to the minimum field necessary to eject ions from a droplet. The true electric field has two maxima of comparable magnitudes: one in a region close the tip of the Taylor cone, known as the "transition region", and the another where the droplets break up from the jet.[12] The total electric field is large at these locations mostly because of the induced field, although there is still a considerable degree of discussion on this point in the literature.[28,45] However, the electric field drops several orders of magnitude when droplets travel further away from the jet break up region. From a device point of view, this variation in the field ensures that the energy is sufficient to extract ions or droplets from the jet but keeps these droplets bounded after they are extruded.

The over prediction of the ion currents in the MD simulations occurs because when a droplet with a single charge breaks apart into ten monomers it generates a factor of 10 higher current. While one droplet carries a large mass with small charge (small $q/m$ ratio), we see that droplets tend to break apart to the smallest entity possible due to high repulsive forces encountered in a droplet breakup.[46] When a droplet breaks apart into multiple monomers a much higher current is generated because monomers travel a lot faster than droplets due to their smaller mass. Since the ionic and total currents include the monomer current, they follow the same trend.

When the electric field is increased further, both the predicted and measured ion currents increase and the magnitude of the predicted current increases faster than the measurements as compared to the lower extrusion voltage. Figure 8 and Figure 9 show the MD currents for applied electric fields of 1.0 and 2.0 V/nm, respectively. For a field of 1.0 V/nm, no droplets are observed, the trimer current is very low, and the dimer current is lower than the measurements. Again, the monomer current is much larger than the measured value because the uniform electric field incorrectly accelerates


dx.doi.org/10.1021/jp402092e | J. Phys. Chem. B 2013, 117, 6768−6781

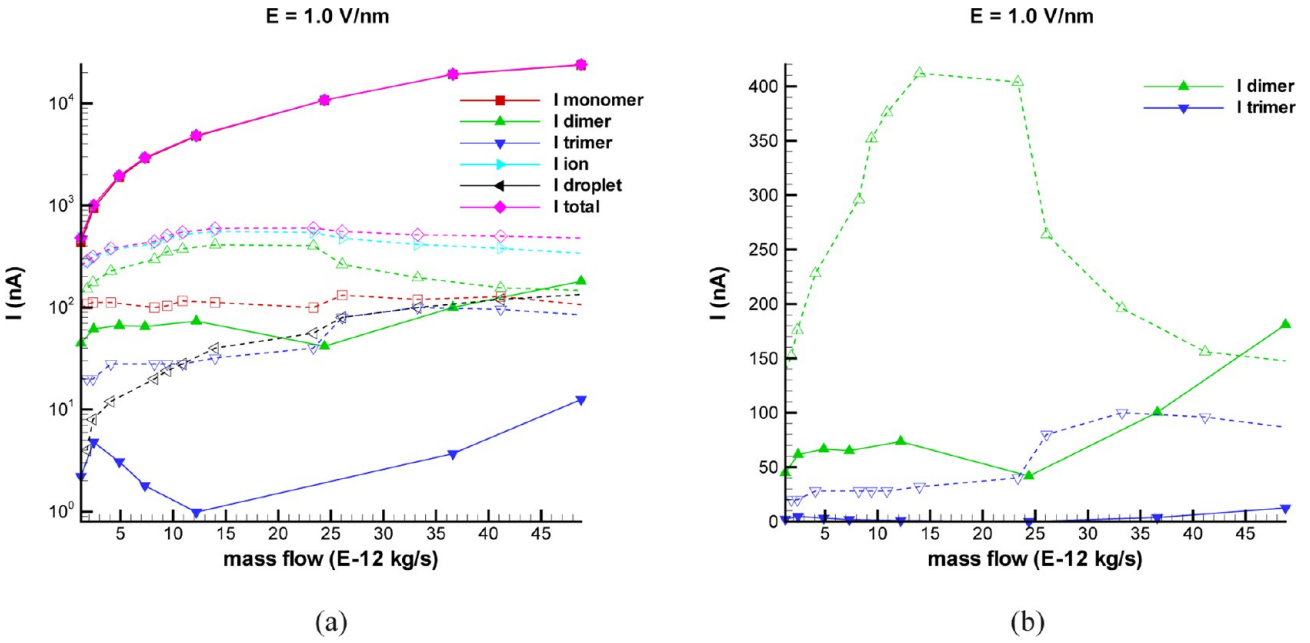


**Figure 8.** Currents as a function of the mass flow rate for the EFCG potential model and applied electric field of 1.0 V/nm. Solid lines represent the calculated currents while dashed lines represents the measured current values from Romero-Sanz et al.[13]

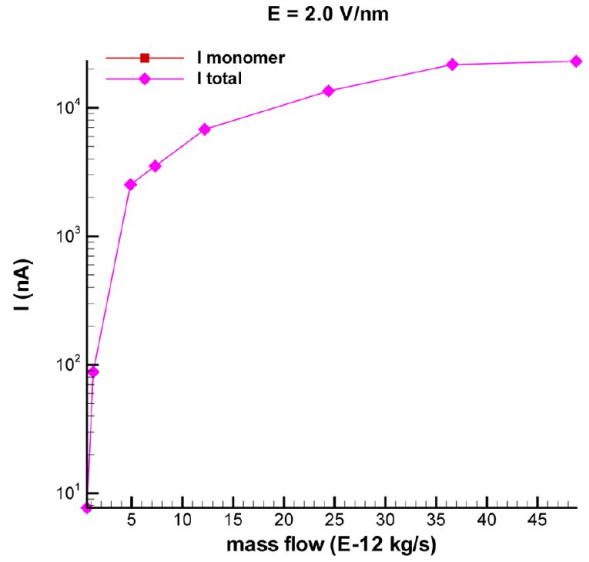


**Figure 9.** Currents as a function of the mass flow rate for the EFCG potential model and applied electric field of 2.0 V/nm.

the droplet break up phenomenon leading to larger currents. For a field of 2.0 V/nm, the simulations predict that only monomers are observed at the virtual extractor. The monomer (or total in this case) current is close to that computed for the 1.0 V/nm field, since the break-up of a few dimers or trimers has a much smaller effect on the total current than the break up of heavy droplets would have, if they were present.

The large increase in the magnitude of the emitted currents predicted by the MD simulations as the extrusion field changes from 0.5 to 2 V/nm can also been seen in the change of the cone-jet structure. Figure 6c shows that at a low flow rate and for an electric field of 2.0 V/nm, the cone-jet has transitioned to a new structure different from that shown in Figure 6a. In the new figure the single well shaped Taylor-cone structure is replaced with multiple emission points, which altogether generate much higher currents than in the single-jet mode of Figure 6a predicted at 0.5 V/nm. An MD simulation with more species would most likely show small, multiple Taylor cones as seen in the work of Cloupeau and Prunet-Foch[8] who call this the "multi-jet mode" of operation. Multijet emission is experimentally observed when the needle (capillary tip) voltage increases past a threshold value that is dependent on the fluid used but is typically on the order of a few thousands of volts. For example, Martinez-Sanchez et al.[43] measured large currents of up to a few thousands nA from a glycerol colloid thruster and distinctly observed that a sharp step-like increase in the current corresponded to the creation of a new jet, up to the point where discrete emission sources where unobservable in a highly stressed regime.

*The Negative Operation Condition.* A negative external electric field was also applied, with the other parameters remaining unchanged and, as expected, negatively charged clusters were emitted from the capillary. For the negative operation condition we present results for $E$ = 0.5 V/nm, the most interesting case discussed previously and where currents of both solvated and nonsolvated ions as well as droplets were found to be present. We consider here the opposite electric field of $E$ = −0.5 V/nm since this case is the most interesting due to the presence of nonsolvated and solvated ions as well as droplets. Figure 10 shows the predicted currents for different mass flow rates for different charged species. The overall trend observed is similar to that observed for the positive electric field. However, negative ions are smaller in size than the cation and therefore require less extraction energy for emission from the capillary. The MD simulations showed that this smaller size leads to a relaxation time generally lower in the negative operation mode. Figure 11 shows a comparison of the measured currents when both polarities of the electric field of magnitude 0.5 V/nm are applied. It can be noticed that the total current produced is slightly higher in the negative operation mode, since the corresponded solvated and non-solvated ions are slightly lighter in this mode (87 amu for the $BF_4^-$ ion vs 111 amu for the $EMIM^+$ ion), leading to higher


dx.doi.org/10.1021/jp402092e | J. Phys. Chem. B 2013, 117, 6768−6781

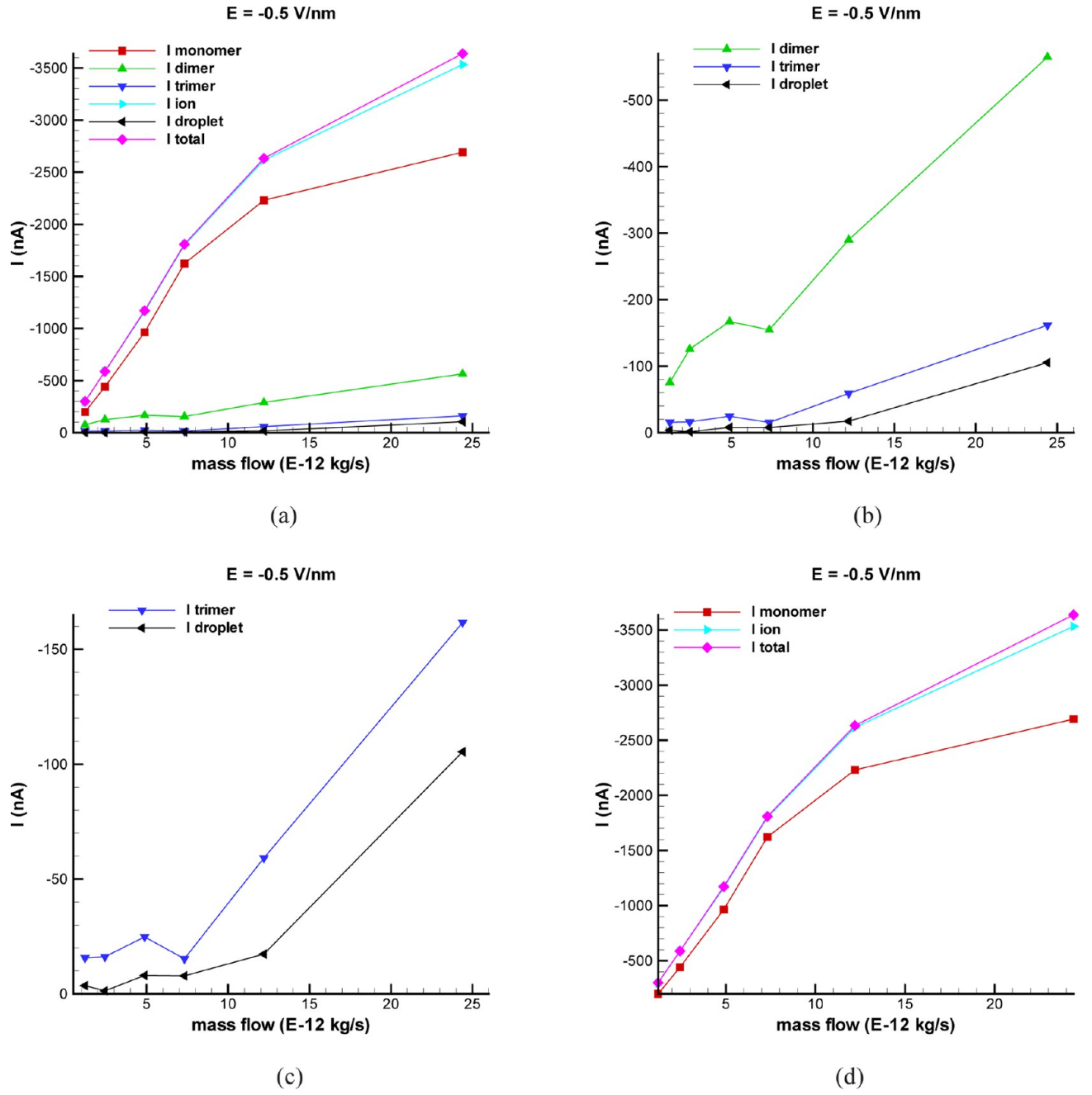


**Figure 10.** Currents as a function of the mass flow rate for the EFCG potential model and applied electric field of −0.5 V/nm.

velocities when extruded. Chiu et al.[14,44] measured currents from a colloid thruster with with the propellants EMIM-Im and EMIM−$BF_4$ in both the positive and negative operation modes and found that for both ILs the current was slightly higher in the negative operation mode. Figure 11 shows that the negative current is slightly higher than the positive one mostly due to the higher contribution of the monomers. The dimer current is actually lower in negative operation mode, while values for the trimer and droplets are almost identical in both operation modes. The ability of MD simulations to interpret and predict these observed trends has important implications for the design of electrospray/colloid thrusters. The similar performance for both polarities opens the possibility of using EMIM−$BF_4$ as the colloid thruster propellant in arrays of emitters, with half positively and negatively biased. The result would be an efficient thruster with no need for a spacecraft neutralizer.

*Thruster Performance.* In order to have an estimate of the suitability of cone jets as colloid thrusters, important propulsive parameters such as the thrust, specific impulse or efficiency can be approximated from eq 2

$$T \approx [2V_A \rho f(\varepsilon)]^{1/2} \left(\frac{K\gamma Q^3}{\varepsilon}\right)^{1/4} \tag{9}$$

$$I_{sp} \approx \left(\frac{1}{g}\right)\left[\frac{2V_A f(\varepsilon)}{\rho}\right]^{1/2}\left(\frac{K\gamma}{Q\varepsilon}\right)^{1/4} \tag{10}$$

where $V_A$ is the thruster acceleration voltage and $g$ is the gravity's acceleration. Generally, for a fixed conductivity, an


dx.doi.org/10.1021/jp402092e | J. Phys. Chem. B 2013, 117, 6768−6781

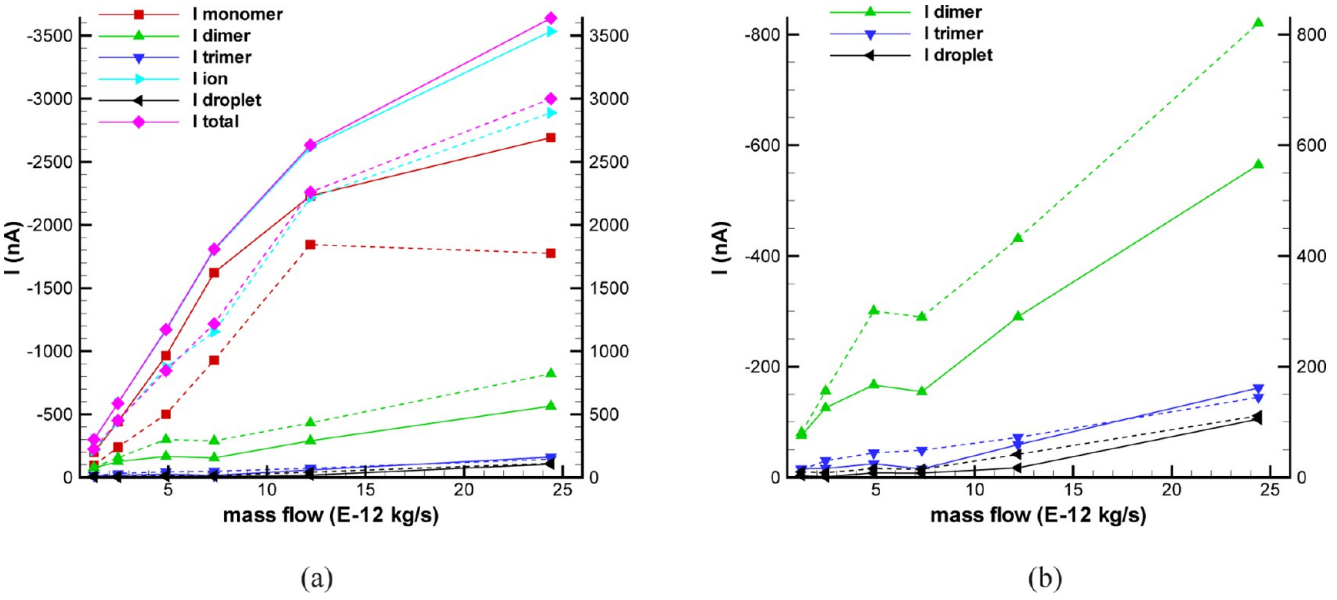


**Figure 11.** Comparison of the currents as a function of the mass flow rate for the EFCG potential model in positive and negative operation modes, for $E$ = 0.5 and −0.5 V/nm. Solid lines represent the positive operation mode while dashed lines represent the negative operation mode.

increase in the flow rate leads to an increase in the thrust, but is penalized by a decrease in the specific impulse. When combining the previous equation with eq 1, it can be seen that the thrust and specific impulse both depend on the electrical conductivity as $T \approx K^{-1/2}$ and $I_{sp} \approx K^{1/2}$. When the emphasis is placed on the specific impulse, it appears it is important to work with propellants of high electrical conductivity. Computationally, the specific impulse can also be estimated using the following relationship

$$I_{sp} = \frac{u'}{g} \tag{11}$$

where $u'$ is the average velocity of the extruded charged cluster at the extraction ring. By combining eqs 5, 9, and 10, the thrust can be estimated from the computed value of the $I_{sp}$ by

$$T = \dot{m} I_{sp} g \tag{12}$$

where $\dot{m}$ is the mass flow rate.

Specific impulse and thrust predicted by the MD simulations were estimated by use of eqs 11 and 12, where $u'$ is the velocity of each cluster in the direction of extrusion. For $E$ = 0.5 V/nm we obtained specific impulses on the order of 475 and 575 s for the positive and negative operation modes, respectively. The corresponding thrust values ranged from 5.7 and 114 and 6.9 and 138 nN, for the positive and negative operation modes, respectively, and for mass flow rates of 1.22 to 24.4 × $10^{-12}$ kg/$m^3$. When the electic field was increased to 1.0 and 2.0 V/nm in the positive operation mode, the $I_{sp}$ increased to 925 and 1465 s and, as expected, the thrust values increased to 11 and 221 and 17.5 and 350 nN respectively, for the same range of mass flow rates. Chiu et al.[14] measured $I_{sp}$ values on the order of 4000 s and thrusts on the order of 36 nN for EMIM−$BF_4$ based on an extraction voltage of ±1500 V, however, they were unable to measure the mass flow rate. Their measured values for the thrust fall in the lower end of our MD results, while the specific impulse we obtained is a factor of 2.75 to 8.5 lower than their measurements. The discrepancy is mostly due to the fact that the net potential modeled in our work is much lower than the one applied by Chiu et al. In our MD simulations, the distance between the tip of the capillary is 862.5 Å, which for electric fields of 0.5, 1.0, and 2.0 V/nm, corresponds to a potential difference, $\Delta\phi$, of 43, 86, and 172.5 V, respectively. We verified that the exit velocity of an emitted charged cluster in the MD simulations is mostly related to the net potential difference by

$$u' = \left(\frac{2e\Delta\phi}{m}\right)^{1/2} \tag{13}$$

Therefore, the lower potential difference in our simulations compared to the experiments leads to a lower estimated specific impulse. The use of a spatially varying homogeneous electric field will be considered in future work.

**Results Obtained using the Simple CG Potential.** To understand the affect of the molecular potential on the IL extrusion process, the extruded ion species, currents, and modes were studied using the simple CG potential model. When an electric field of 0.5 V/nm was applied, it was found that no ions or droplets were emitted from the capillary for any mass flow. Figure 12a shows the simple jet emitted from the capillary for a mass flow of 24.4 × $10^{-12}$ kg/s. It is similar to the "simple jet" operating mode described by Cloupeau and Prunet-Foch,[8] in a case where the electric field is too low and the mass flow high enough to form a jet of separated, charged ions and ion clusters. We see in the simulation that as the IL leaves the capillary it retains its "bulk", uncharged liquid structure and remains collimated with the same radius as the capillary. The intermolecular forces are seen to be too strong to extract separate ions from the bulk and therefore no current will be generated by the extractor for this system.

Ion and droplet emission was obtained when the electric field was increased. An electric field of 1.0 V/nm generates currents, but the conditions are still close to a dripping mode that becomes unstable and breaks up into smaller ions and droplets. Figure 12b shows a close-up view of a cone-jet and its breakup region and it can be seen that ions and small droplets are emitted off the tip of the cone. The currents calculated for fields of 1.0 and 2.0 V/nm are plotted in Figure 13 and Figure 14, respectively. Small droplets are present at 1.0 V/nm, but have


dx.doi.org/10.1021/jp402092e | J. Phys. Chem. B 2013, 117, 6768−6781

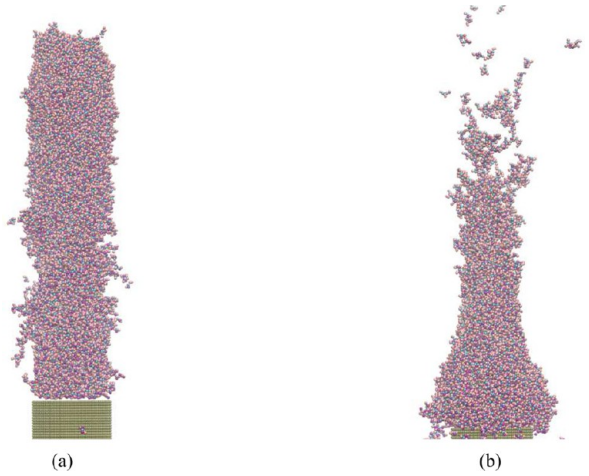


**Figure 12.** Two typical electrospray jets observed for the simple CG potential. Vertical dimension corresponds to 400 Å.

completely disappeared for a field of 2.0 V/nm. The proportion of dimer and trimers has also been reduced when the field was doubled. The calculated currents are much lower for the simple CG potential than the EFCG potential for the same electric field and the multijet mode emission is not observed. The ion current trends for the simple CG systems at 1.0 and 2.0 V/nm are similar to that of the EFCG systems at 0.5 and 1.0 V/nm, respectively, but it takes an electric field twice the strength of the one applied to the EFCG system to emit clusters from the simple CG system. The interatomic potential that causes the simple CG system to equilibrate at a density twice the value measured experimentally and obtained by the EFCG potential also requires an external energy source twice the value measured to generate ion extrusion.

## CONCLUSIONS AND FUTURE WORK

Molecular Dynamics simulations were performed to model an ionic liquid electrospray thruster. First, the impact of the coarse-grained model on the IL EMIM−$BF_4$ was studied. Two cubic systems were equilibrated with periodic boundary conditions. The system based on the EFCG potential leads to a density equal the measured value and radial distribution functions in agreement with the ones for a full-atom model, while the simple CG potential showed substantial discrepancies and the formation of "bubbles" was visually observed. A system modeling an electrospray, IL capillary was then equilibrated for both CG potentials, and an extrusion model was developed based on a repulsive wall potential to simulate a constant mass flow inside the capillary. Multiple electric fields were applied to the system and the mass flow rate was also varied. Three ionic species, monomers, dimers and trimers, as well as droplets were observed and their current distributions were recorded at a distance of 0.1 $\mu$m from the center of the capillary.

The MD simulations of the extruded IL demonstrated at an atomistic level a number of the features that have been measured in many experiments. The formation of a Taylor cone was observed directly from the MD simulations for the first time when the simulated mass flow was sufficiently high. The features of the MD simulations results using the EFCG potential agreed best with experiments for an electric field of 0.5 V/nm, where solvated ions and droplets were observed and the computed currents provided reasonable agreement with the values measured by Romero et al.,[13] especially at low mass flow rates. When the mass flow rate increased, larger droplets tended to break apart, leading to an increase in the predicted monomer current. For higher values of the electric field, the MD simulations predicted that almost exclusively monomers would be extruded and that the predicted overestimate of the current occurs because the IL has a multijet mode structure.

Similar computations were performed using the simple CG potential model. Application of an electric field of 0.5 V/nm showed that no current was generated, while higher electric

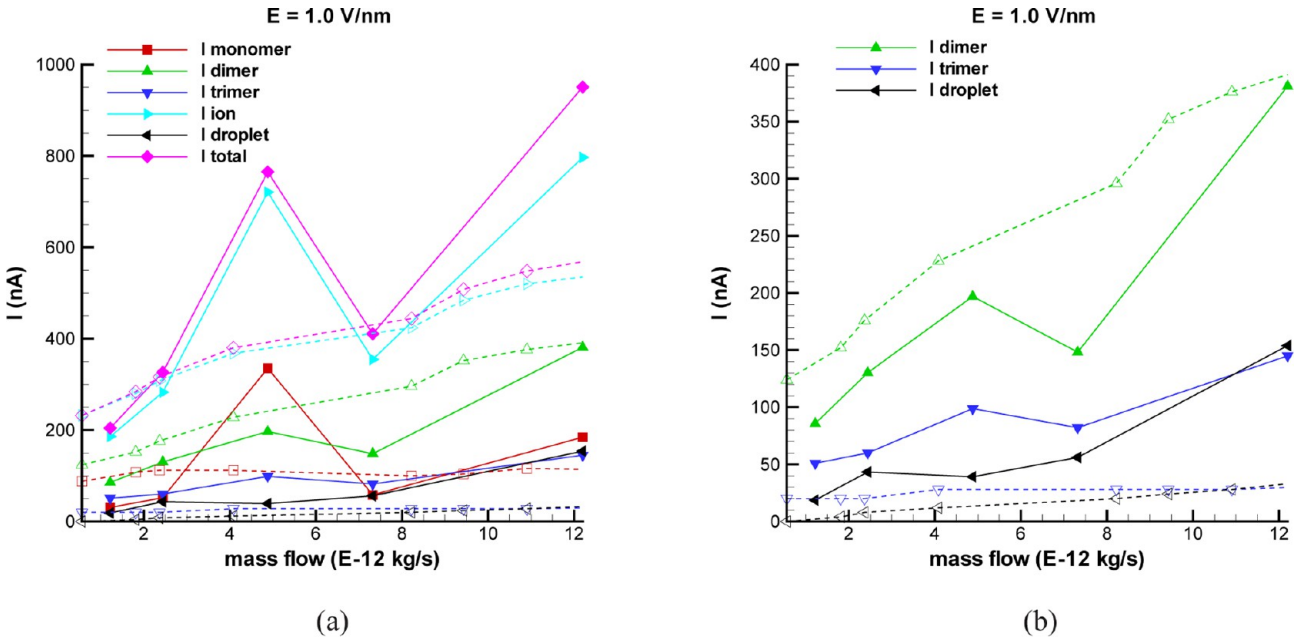


**Figure 13.** Currents as a function of the mass flow rate for the simple CG potential model and applied electric field of 1.0 V/nm. Solid lines represent the calculated currents while dashed lines represents the measured current values from Romero-Sanz et al.[13]


dx.doi.org/10.1021/jp402092e | J. Phys. Chem. B 2013, 117, 6768−6781

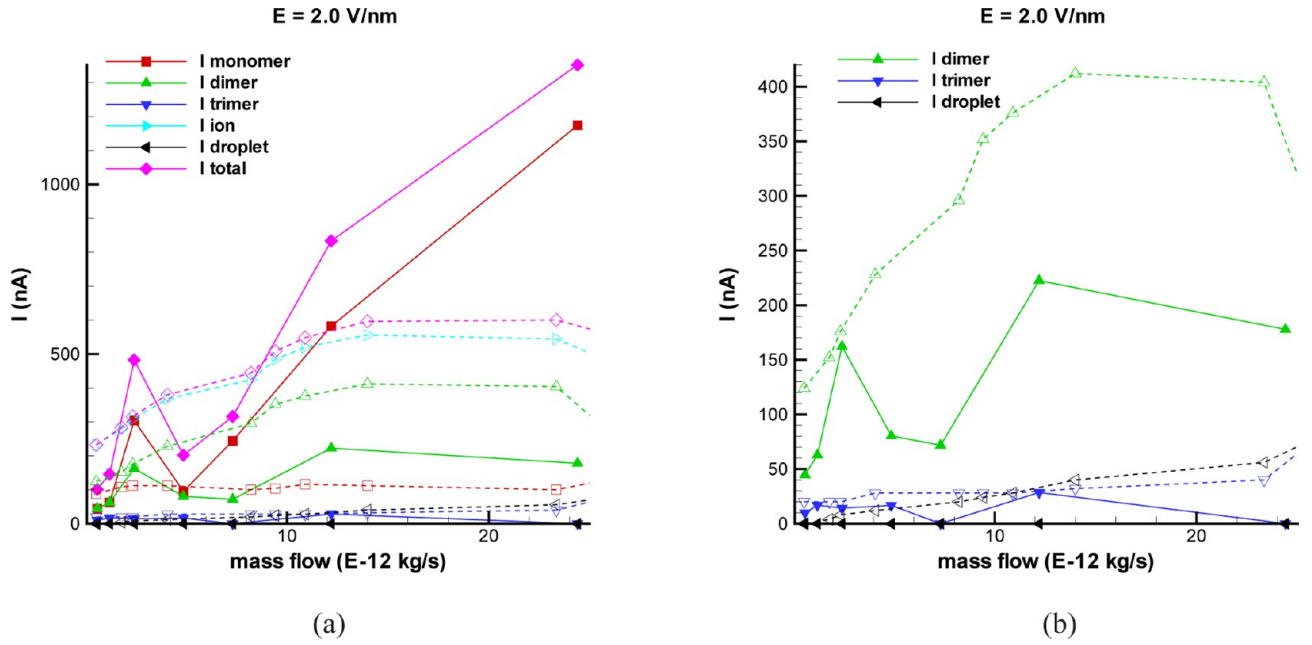


**Figure 14.** Currents as a function of the mass flow rate for the simple CG potential model and applied electric field of 2.0 V/nm. Solid lines represent the calculated currents while dashed lines represents the measured current values from Romero-Sanz et al.[13]

fields of 1.0 and 2.0 V/nm led to computed current values similar to these of the EFCG potential at fields of 0.5 and 1.0 V/nm, respectively. This result is consistent with the fact that the simple CG potential model overestimates the intermolecular forces which, in turn, predicts the wrong IL density and requires a higher external energy to extrude charged particles, compared to the EFCG model. A definitive statement cannot be made at this point as to which molecular potential model is better in the nonequilibrium, extrusion MD simulations because we cannot match the experimental local electric fields.

While not the main emphasis of this work, a number of results obtained from the MD simulations support trends that are related to device performance. When the polarity was reversed, similar results for the anion currents were obtained, paving the way for the use of for the use of EMIM−$BF_4$ as an efficient propellant for arrays of emitters with switching polarity neutralizing strategies. Thrust and specific impulses were estimated based on the exit velocities of charged clusters and the estimated thrust was generally found to be in good agreement with the measured values while the specific impulses were underestimated. The implementation of a spatially varying electric field that adapts to the IL space charge presence should help shed more light on these discrepancies. Additional experimental work that better characterizes both the IL mass flow rate as well as the actual electric field at the tip will also provide better insight into the physics of IL extrusion at the atomistic level.

## AUTHOR INFORMATION

### Corresponding Author

*E-mail: dalevin@psu.edu. Phone: +1 (814) 865-6435. Fax: +1 (814) 865-6435.

### Notes

The authors declare no competing financial interest.

## ACKNOWLEDGMENTS

The research being performed at the Pennsylvania State University is supported by the Air Force Office of Scientific Research through the MACEEP Grant No. FA9550-09-1-0695, whose support is gratefully acknowledged. The authors are grateful to John Daily for providing the DL_POLY[32] tabulated potential input file for the EFCG potential.

## REFERENCES

(1) Chiarot, P.; Sullivan, P.; Mrad, R. B. An Overview of Electrospray Applications in MEMS and Microfluidic Systems. *J. Microelectromech. Syst.* **2011**, *20*, 1241−1249.
(2) Luedtke, W.; Landman, U.; Chiu, Y.; Levandier, D.; Dressler, R.; Sok, S.; Gordon, M. Nanojets, Electrospray, and Ion Field Evaporation: Molecular Dynamics Simulations and Laboratory Experiments. *J. Phys. Chem. A* **2008**, *112*, 9628−9649.
(3) Taylor, G. I. Disintegration of Water Drops in an Electric Field. *Proc. R. Soc. London, Ser. A* **1964**, *280*, 383−397.
(4) Krohn, V. *Liquid Metal Droplets for Heavy Particle Propulsion*; A. C. Press: New York and London, 1961; Vol. *5*, pp 73−80.
(5) Krohn, V. *Glycerol Droplets for Electrostatic Propulsion*; ARS Electric Propulsion Conf., Berkeley, CA, 1962.
(6) Mueller, J. Thruster Options for Microspacecraft: a Review and Evaluation of State-of-the- Art and Emerging Technologies. *Prog. Astronaut. Aeronaut.* **2000**, *187*, 45−138.
(7) Prewett, P. D.; Mair, G. L. R. Focused Ion Beams from Liquid Metal Ion Sources. *Surf. Interface Anal.* **1992**, *18*, 377−377.
(8) Cloupeau, M.; Prunet-Foch, B. Electrostatic Spraying of Liquids: Main Functioning Modes. *J. Electrostat.* **1990**, *25*, 165−184.
(9) De La Mora, J. F.; Loscertales, I. G. The Current Emitted by Highly Conducting Taylor Cones. *J. Fluid Mech.* **1994**, *260*, 155−184.
(10) Martinez-Sanchez, M. Lecture 23−25: Colloidal Engines. Appendix, 2004.
(11) Gamero-Castano, M.; Hruby, V. Electrospray as a Source of Nanoparticles for Efficient Colloid Thrusters. *J. Propul. Power* **2001**, *17*, 977−987.
(12) Gamero-Castano, M. Electric-Field-Induced Ion Evaporation from Dielectric Liquid. *Phys. Rev. Lett.* **2002**, *89*, 147602.
(13) Romero-Sanz, I.; Bocanegra, R.; Fernandez de la Mora, J.; Gamero-Castano, M. Source of Heavy Molecular Ions Based on Taylor

Cones of Ionic Liquids Operating in the Pure Ion Evaporation Regime. *J. Appl. Phys.* **2003**, *94*, 3599−3605.
(14) Chiu, Y.; Austin, B.; Dressler, R.; Levandier, D.; Murray, P.; Lozano, P.; Katz, I.; de la Mora, J.; Sanchez, M. Mass Spectrometric Analysis of Colloid Thruster Ion Emission from Selected Propellants. *J. Propul. Power* **2005**, *21*, 416−423.
(15) Carretero, J.; Martinez-Sanchez, M. Numerical Simulation of a Colloidal Thruster in the Droplet Regime. *Comput. Phys. Commun.* **2004**, *164*, 202−208.
(16) Herrada, M. A.; López-Herrera, J. M.; Gañán Calvo, A. M.; Vega, E. J.; Montanero, J. M.; Popinet, S. Numerical Simulation of Electrospray in the Cone-Jet Mode. *Phys. Rev. E* **2012**, *86*, 026305.
(17) de Andrade, J.; Boes, E. S.; Stassen, H. Computational Study of Room Temperature Molten Salts Composed by 1-Alkyl-3-methyl-imidazolium Cations Force-Field Proposal and Validation. *J. Phys. Chem. B* **2002**, *106*, 13344−13351.
(18) Cornell, W. D.; Cieplak, P.; Bayly, C. I.; Gould, I. R.; Merz, K. M.; Ferguson, D. M.; Spellmeyer, D. C.; Fox, T.; Caldwell, J. W.; Kollman, P. A. A Second Generation Force Field for the Simulation of Proteins, Nucleic Acids, and Organic Molecules. *J. Am. Chem. Soc.* **1995**, *117*, 5179−5197.
(19) Takahashi, N.; Lozano, P. C. Computational Investigation of Molecular Ion Evaporation in Electrospray Thrusters. 44th AIAA/ASME/SAE/ASEE Joint Propulsion Conference and Exhibit, Hartford, CT, July 21−23 2008, AIAA−2008−4533.
(20) Daily, J. W.; Micci, M. M. Ionic Velocities in an Ionic Liquid under High Electric Fields using All-Atom and Coarse-Grained Force Field Molecular Dynamics. *J. Chem. Phys.* **2009**, *131*, 094501.
(21) Wang, Y.; Izvekov, S.; Yan, T.; Voth, G. A. Multiscale Coarse-Graining of Ionic Liquids. *J. Phys. Chem. B* **2006**, *110*, 3564−3575.
(22) Wang, Y.; Noid, W. G.; Liu, P.; Voth, G. A. Effective Force Coarse-Graining. *Phys. Chem. Chem. Phys.* **2009**, *11*, 2002−2015.
(23) Borner, A.; Li, Z.; Levin, D. Modeling of an Ionic Liquid Electrospray using Molecular Dynamics with Constraints. *J. Chem. Phys.* **2012**, *136*, 124507.
(24) Garoz, D.; Bueno, C.; Larriba, C.; Castro, S.; Romero-Sanz, I.; Fernandez de La Mora, J.; Yoshida, Y.; Saito, G. Taylor Cones of Ionic Liquids from Capillary Tubes as Sources of Pure Ions: The Role of Surface Tension and Electrical Conductivity. *J. Appl. Phys.* **2007**, *102*, 064913−064913.
(25) Terhune, K.; King, L. Ion and Droplet Mass Measurements of an Electrospray Emitter using an ExB Filter. 32nd International Electric Propulsion Conference, 11−15 September 2011, Wiesbaden, Germany, 2011, IEPC−2011−299.
(26) de la Mora, J. F. On the Outcome of the Coulombic Fission of a Charged Isolated Drop. *J. Colloid Interface Sci.* **1996**, *178*, 209−218.
(27) Grimm, R. L.; Beauchamp, J. L. Dynamics of Field-Induced Droplet Ionization: Time- Resolved Studies of Distortion, Jetting, and Progeny Formation from Charged and Neutral Methanol Droplets Exposed to Strong Electric Fields. *J. Phys. Chem. B* **2005**, *109*, 8244−8250.
(28) de La Mora, F. The Fluid Dynamics of Taylor Cones. *Annu. Rev. Fluid Mech.* **2007**, *39*, 217−243.
(29) Gamero-Castano, M.; de laMora, J. F. Direct Measurement of Ion Evaporation Kinetics from Electrified Liquid Surfaces. *J. Chem. Phys.* **2000**, *113*, 815−832.
(30) Andersen, H. C. Rattle: A "Velocity" Version of the Shake Algorithm for Molecular Dynamics Calculations. *J. Comput. Phys.* **1983**, *52*, 24−34.
(31) Daily, J. Private Communication, 2012.
(32) Todorov, I.; Smith, W.; Trachenko, K.; Dove, M. DL_POLY_3: New Dimensions in Molecular Dynamics Simulations via Massive Parallelism. *J. Mater. Chem.* **2006**, *16*, 1911−1918.
(33) Nose, S. A Molecular Dynamics Method for Simulations in the Canonical Ensemble. *Mol. Phys.* **1984**, *52*, 255−268.
(34) Hoover, W. G. Canonical Dynamics: Equilibrium Phase-Space Distributions. *Phys. Rev. A* **1985**, *31*, 1695−1697.
(35) Melchionna, S.; Ciccotti, G.; Lee Holian, B. Hoover NPT Dynamics for Systems Varying in Shape and Size. *Mol. Phys.* **1993**, *78*, 533−544.
(36) Martyna, G. J.; Tobias, D. J.; Klein, M. L. Constant Pressure Molecular Dynamics Algorithms. *J. Chem. Phys.* **1994**, *101*, 4177−4189.
(37) Essmann, U.; Perera, L.; Berkowitz, M. L.; Darden, T.; Lee, H.; Pedersen, L. G. A Smooth Particle Mesh Ewald Method. *J. Chem. Phys.* **1995**, *103*, 8577−8593.
(38) Allen, M. P.; Tildesley, D. J. *Computer Simulation of Liquids*; Clarendon Press: Oxford, 1989.
(39) Del Popolo, M. G.; Voth, G. A. On the Structure and Dynamics of Ionic Liquids. *J. Phys. Chem. B* **2004**, *108*, 1744−1752.
(40) Wolf, D.; Keblinski, P.; Phillpot, S. R.; Eggebrecht, J. Exact Method for the Simulation of Coulombic Systems by Spherically Truncated, Pairwise r Summation. *J. Chem. Phys.* **1999**, *110*, 8254−8282.
(41) Israelachvili, J. *Intermolecular and Surface Forces*; Academic, New York, 1992.
(42) Hayashi, T.; Pertsin, A. J.; Grunze, M. Grand Canonical Monte Carlo Simulation of Hydration Forces Between Nonorienting and Orienting Structureless Walls. *J. Chem. Phys.* **2002**, *117*, 6271−6280.
(43) Martinez-Sanchez, M.; de la Mora, J. F.; Hruby, V.; Gamero-Castano, M.; Khayms, V. Research on Colloid Thrusters. 26th International Electric Propulsion Conference, Kitakyushu, Japan, 1999, IEPC−99−014.
(44) Chiu, Y.-H.; Gaeta, G.; Levandier, D.; Dressler, R.; Boatz, J. Vacuum Electrospray Ionization Study of the Ionic Liquid, [Emim]-[Im]. *Int. J. Mass Spectrom.* **2007**, *265*, 146−158.
(45) Gañán Calvo, A.; Montanero, J. Revision of Capillary Cone-Jet Physics: Electrospray and Flow Focusing. *Phys. Rev. E* **2009**, *79*, 066305−1−066305−18.
(46) Gomez, A.; Tang, K. Charge and Fission of Droplets in Electrostatic Sprays. *Phys. Fluids* **1994**, *6*, 404−414.